



**Nanocrystalline and Ultra-Fine Grained Tungsten for  
Kinetic Energy Penetrator and Warhead  
Liner Applications**

**by Kyu Cho, Laszlo Kecskes, Robert Dowding, Brian Schuster,  
Qiuming Wei, and Ruslan Z. Valiev**

**ARL-RP-180**

**June 2007**

*A reprint from the Proceedings of the 25th Army Science Conference, Orlando, FL, 27 November 2006.*

## **NOTICES**

### **Disclaimers**

The findings in this report are not to be construed as an official Department of the Army position unless so designated by other authorized documents.

Citation of manufacturer's or trade names does not constitute an official endorsement or approval of the use thereof.

Destroy this report when it is no longer needed. Do not return it to the originator.

# **Army Research Laboratory**

Aberdeen Proving Ground, MD 21005-5069

---

---

**ARL-RP-180**

**June 2007**

---

---

## **Nanocrystalline and Ultra-Fine Grained Tungsten for Kinetic Energy Penetrator and Warhead Liner Applications**

**Kyu Cho, Laszlo Kecskes, Robert Dowding, and Brian Schuster**  
Weapons and Materials Research Directorate, ARL

**Qiuming Wei**  
University of North Carolina

**Ruslan Z. Valiev**  
Ufa State Aviation Technical University

*A reprint from the Proceedings of the 25th Army Science Conference, Orlando, FL, 27 November 2006.*

REPORT DOCUMENTATION PAGE			Form Approved OMB No. 0704-0188		
Public reporting burden for this collection of information is estimated to average 1 hour per response, including the time for reviewing instructions, searching existing data sources, gathering and maintaining the data needed, and completing and reviewing the collection information. Send comments regarding this burden estimate or any other aspect of this collection of information, including suggestions for reducing the burden, to Department of Defense, Washington Headquarters Services, Directorate for Information Operations and Reports (0704-0188), 1215 Jefferson Davis Highway, Suite 1204, Arlington, VA 22202-4302. Respondents should be aware that notwithstanding any other provision of law, no person shall be subject to any penalty for failing to comply with a collection of information if it does not display a currently valid OMB control number. <b>PLEASE DO NOT RETURN YOUR FORM TO THE ABOVE ADDRESS.</b>					
1. REPORT DATE (DD-MM-YYYY) June 2007		2. REPORT TYPE Reprint		3. DATES COVERED (From - To) 1 October 2005–30 September 2006	
4. TITLE AND SUBTITLE Nanocrystalline and Ultra-Fine Grained Tungsten for Kinetic Energy Penetrator and Warhead Liner Applications			5a. CONTRACT NUMBER		
			5b. GRANT NUMBER		
			5c. PROGRAM ELEMENT NUMBER		
6. AUTHOR(S) Kyu Cho, Laszlo Kecskes, Robert Dowding, Brian Schuster, Qiuming Wei,* and Ruslan Z. Valiev†			5d. PROJECT NUMBER 62105H84, 62618H80		
			5e. TASK NUMBER		
			5f. WORK UNIT NUMBER		
7. PERFORMING ORGANIZATION NAME(S) AND ADDRESS(ES) U.S. Army Research Laboratory ATTN: AMSRD-ARL-WM-MB Aberdeen Proving Ground, MD 21005-5069			8. PERFORMING ORGANIZATION REPORT NUMBER ARL-RP-180		
9. SPONSORING/MONITORING AGENCY NAME(S) AND ADDRESS(ES)			10. SPONSOR/MONITOR'S ACRONYM(S)		
			11. SPONSOR/MONITOR'S REPORT NUMBER(S)		
12. DISTRIBUTION/AVAILABILITY STATEMENT Approved for public release; distribution is unlimited.					
13. SUPPLEMENTARY NOTES A reprint from the <i>Proceedings of the 25th Army Science Conference</i> , Orlando, FL, 27 November 2006. *University of North Carolina at Charlotte, Mechanical Engineering Department, Charlotte, NC 28223-0001 †Institute of Physics of Advanced Materials, Ufa State Aviation Technical University, Ufa 450000, Russia					
14. ABSTRACT For the first time, we have demonstrated adiabatic shear localization in pure, ultra-fine grain (UFG) and nanocrystalline (NC) tungsten (W). Fabricated by severe plastic deformation (SPD), microstructural and mechanical property analyses of the W samples show that the combination of fine grain size, stored strain energy, ultra-high strength, little or no work hardening capacity leads to a unique flow softening behavior. It is further hypothesized that, while maintaining material ductility, grain refinement and redistribution of pre-existing impurities, segregated along grain boundaries (GBs), are equally critical for localized flow softening to occur.  The UFG and SPD W results serve as minimum property benchmarks for shear localization to occur. In turn, these are used to define the experimental protocols and parameters for use in alternate fabrication procedures such as rapid consolidation of UFG or NC W powders. Preliminary results indicate that additional development of high-purity W nanopowders and appropriate grain-growth inhibitors will be required for this latter approach to successfully produce UFG and NC W microstructures.					
15. SUBJECT TERMS nanomaterials, tungsten, consolidation, severe plastic deformation, materials processing					
16. SECURITY CLASSIFICATION OF:			17. LIMITATION OF ABSTRACT UL	18. NUMBER OF PAGES 14	19a. NAME OF RESPONSIBLE PERSON Kyu Cho
a. REPORT UNCLASSIFIED	b. ABSTRACT UNCLASSIFIED	c. THIS PAGE UNCLASSIFIED			19b. TELEPHONE NUMBER (Include area code) (410) 306-0820

# NANOCRYSTALLINE AND ULTRA-FINE GRAINED TUNGSTEN FOR KINETIC ENERGY PENETRATOR AND WARHEAD LINER APPLICATIONS

Kyu Cho,\* Laszlo Kecskes, Robert Dowding, and Brian Schuster  
U.S. Army Research Laboratory, Weapons and Materials Research Directorate  
AMSRD-ARL-WM-MB, Aberdeen Proving Ground, MD 21005-5069

Qiuming Wei  
University of North Carolina at Charlotte, Mechanical Engineering Department  
9201 University City Boulevard, Charlotte, NC 28223-0001

Ruslan Z. Valiev  
Institute of Physics of Advanced Materials, Ufa State Aviation Technical University  
12 Karl Marx Street, Ufa 450000, Russia

## ABSTRACT

For the first time, we have demonstrated adiabatic shear localization in pure, ultra-fine grain (UFG) and nanocrystalline (NC) tungsten (W). Fabricated by severe plastic deformation (SPD), microstructural and mechanical property analyses of the W samples show that the combination of fine grain size, stored strain energy, ultra-high strength, little or no work hardening capacity leads to a unique flow softening behavior. It is further hypothesized that, while maintaining material ductility, grain refinement and redistribution of pre-existing impurities, segregated along grain boundaries (GBs), are equally critical for localized flow softening to occur.

The UFG and SPD W results serve as minimum property benchmarks for shear localization to occur. In turn, these are used to define the experimental protocols and parameters for use in alternate fabrication procedures such as rapid consolidation of UFG or NC W powders. Preliminary results indicate that additional development of high-purity W nanopowders and appropriate grain-growth inhibitors will be required for this latter approach to successfully produce UFG and NC W microstructures.

## 1. INTRODUCTION

Recent interest in materials with UFG,  $\sim 100$  nm  $<$  grain size,  $d < \sim 500$  nm, or NC,  $d < 100$  nm, size regimes has been tremendous (Meyers et al., 2006; Witkin and Lavernia, 2006). These materials have much higher strengths compared to their coarse-grained (CG) counterparts. However, such high strengths have been accompanied by loss of ductility (Koch, 2003; Ma, 2003a, 2003b). Instead of being an intrinsic property, it has been proposed that the loss of ductility is a defect-induced phenomenon (Youssef et al., 2005; Cheng et al., 2005; Wang and Ma, 2004; Wang et al., 2002). Probable causes are linked to volume defects, such as residual porosity and poor interparticle bonding that stem from impurity contamination. These defects are introduced during “two-

step” processes, wherein UFG/NC structures are produced by ultrafine powder compaction at high temperatures (Wei et al., 2006b). To avoid such complications, “one-step” processes have been pursued, wherein powder handling in air is minimized or the precursor is in a fully dense bulk form. Examples are known as “in-situ” consolidation (Youssef et al., 2005) and SPD (Valiev et al., 2000), respectively.

Recent UFG/NC fabrication efforts have been on face-centered-cubic (FCC) metals such as Al, Cu, or Ni (Kumar et al., 2003). Much less work exists on body-centered-cubic (BCC) metals, e.g., W or Fe. UFG/NC BCC metals have different properties than their FCC counterparts (Wei et al., 2002, 2003, 2004a, 2004b, 2004c, 2006a, 2006c; Malow and Koch, 1998; Malow et al., 1998; Carsley et al., 1998). For example, UFG/NC Fe exhibits localized shearing even under quasi-static uniaxial compression (Wei et al., 2002; Jia et al., 2003). NC V fails in a manner similar to metallic glass under dynamic uniaxial compression (Wei et al., 2004b). Such behavior is based on the vanishing strain hardening and much reduced strain rate sensitivity (SRS). This deformation and failure mode is highly desirable in kinetic energy projectile applications (Magness et al., 1995).

Plastic instability is typically manifested when the stabilizing mechanisms (strain and strain rate hardening) are diminished and the destabilizing mechanisms (thermal and geometric flow softening) dominate (Wright, 2002; Bai and Dodd, 1992). It has been shown that as  $d$  decreases for BCC metals, the strain hardening capacity disappears, the SRS diminishes (Jia et al., 2003; Wei et al., 2004c, 2006a, 2006c), and flow softening behavior begins to dominate. In agreement with previously proposed flow softening (Jonas et al., 1976) and adiabatic shear banding (ASB) criteria (Wright, 2002), it is expected that localized flow softening behavior may occur if the grain size of W is reduced to UFG or NC (Wei et al., 2006a, 2006c) scale.

In general, there are two routes for fabricating bulk UFG and NC W, namely, top-down and bottom-up approaches. In the former, the original bulk CG structure, subjected to SPD, is broken down and refined into a UFG or NC structure (Valiev et al., 2000). In contrast, in the latter approach, the fine-grained structure is created using a “two-step” process in which nanosized precursor powders are consolidated into a fully dense structure. Control of grain size, however, is a difficult task because heat, necessary for consolidation and densification, promotes grain boundary (GB) diffusion that naturally encourages grain growth (Rieck, 1967; Cho et al., 2004). To limit grain growth, extremely rapid heating rates, with no (or very short) soak time, are preferred. Application of high pressure is also desirable as it provides additional driving force for densification.

We demonstrate the use of the top-down approach to produce pure UFG- and NC-W materials. The UFG structure was achieved by equi-channel angular pressing (ECAP) followed by warm rolling. The UFG structure was further refined to NC structure by a high-pressure torsion (HPT) technique (Zhilyaev et al., 2003). The compressive mechanical properties were collected at quasi-static and at high strain rates. Transmission and scanning electron microscopies (TEM/SEM) were used to evaluate the extent of plastic deformation, shear localization, and failure mechanisms.

Very few ultra-fine W powders are available; their lot-to-lot purity, high oxygen content, and size distribution are not reliable. In contrast, sub-micron W is sold commercially. Therefore, we present experimental parameters developed for the densification of such powders using an electric discharge powder consolidation method, also known as, plasma pressure compaction (P<sup>2</sup>C) (Groza, 1998, Yoo et al., 1999). The intent is to establish a baseline for the consolidation of UFG- and NC-W powders. Because of the two-step nature of the P<sup>2</sup>C process, we kept powder handling in air to a minimum. W compacts were consolidated to near full density and characterized by X-ray diffraction, SEM and energy dispersive X-ray spectroscopy (EDXS). Special attention was given to reveal potential oxygen containing phase(s) along the GBs.

## 2. EXPERIMENTAL PROCEDURES

### 2.1. Top-Down Approach

Table I. Interstitial Impurities of the Starting W

Element	C	H	N	O	P	S	Si
( $\mu\text{g/g}$ ; or ppm)	30	5	5	20	20	5	20

A wrought W bar, with a grain size of  $\sim 40 \mu\text{m}$ , supplied by Plansee AG, (Reutte, Austria), was used as a

starting material for SPD. Table I summarizes vendor certified chemical analyses of interstitial impurities.

#### 2.1.1. ECAP and Rolling Preparation of UFG W

The W bar was passed through an ECAP tool with a set of interconnecting channels of equal cross-sectional areas and shapes. Extrusion was performed at  $1000 \text{ }^\circ\text{C}$ . The reason for this low temperature is because above  $1250 \text{ }^\circ\text{C}$ , rapid recrystallization takes place in deformed W (Farrell et al., 1967). The recrystallization temperature is a strong function of impurity level and the amount of plastic deformation (Lassner and Schubert, 1998). The work piece was encapsulated in a stainless steel can to reduce oxidation. Due to the relatively poor workability of CG W, a  $120^\circ$  die angle was used to avoid cracking. Compared to a right-angle tool, the effective strain introduced through each pass is reduced. This could be compensated for by increasing the number of passes.

To further refine the W microstructure, a section was machined off the ECAP bar and rolled in a confined manner at successively lower temperatures from  $800$  to  $600 \text{ }^\circ\text{C}$ . The rolling plane was perpendicular to the ECAP extrusion direction. The additional equivalent von Mises strain introduced through this rolling process was about 1.8. The W that was subjected to ECAP followed by rolling will be referred to as UFG W.

#### 2.1.2. HPT Preparation of NC W

Polished W disks, 10-mm diameter and 1-mm thick, were confined under pressure while subjected to a torsional force for five turns. No apparent change in color of the W piece was observed suggesting no oxidation during processing. The HPT temperature,  $500 \text{ }^\circ\text{C}$ , was far below the melting point or recrystallization temperature of W, so the microstructure was likely refined. The strain induced in the work piece is radially dependent. The rim of the disk subjected to one complete HPT turn has a von Mises equivalent strain of  $>18$ . Thus, after five turns, the maximum nominal strain was about 90. The W sample subjected to HPT will be referred to as NC W.

#### 2.1.3. Microstructural Analyses

TEM specimens were cut from the ECAP extrudates and HPT disks such that the electron beam was in the plane of the rod and disk, respectively. The specimens were first mechanically polished down to  $\sim 50 \mu\text{m}$  thick then dimpled. The dimpled specimen was mounted on a Ta support grid and ion milled to electron transparency. A Philips EM420 TEM operated at 120 kV was used for conventional analysis, while a Philips CM-300, TEM operated at 300 kV was used for high-resolution lattice imaging. For some recovered samples, the roughened

side faces were polished away and chemically etched to expose the structure of the shear bands.

#### 2.1.4. Mechanical Testing

Samples for quasi-static and dynamic mechanical testing were machined from the SPD processed W. An MTS servo-hydraulic mechanical testing system was used to measure the quasi-static behavior at strain rates of  $10^{-4}$  to  $10 \text{ s}^{-1}$ . The compressive loading direction was along the ECAP extrusion direction, normal to the rolling plane of the rolled samples, and normal to the torsion plane of the HPT samples. A standard Kolsky bar and a desk-top Kolsky bar were used to measure the dynamic behavior. The side faces of the specimens were polished to a mirror finish. Specimens were recovered for optical and SEM observation of post-loaded samples for evidence of localized shearing and failure surface morphology.

## 2.2. Bottom-Up Approach

### 2.2.1. Precursor Characterization

Tables II and III summarize vendor specifications and chemical analysis of the starting W powder. Particle size distribution of the W powder was determined by laser scattering, using a 50/50 vol.% glycerol and  $\text{H}_2\text{O}$  dispersant mixture. Initial W powder chemistry was verified by inert gas fusion and its morphology verified by SEM.

Table II. Vendor Specification of the Starting W Powder

Vendor	Grade	PSR	Purity	LOR
Osram Sylvania	M10	0.60-0.90	99.95%	0.4%

PSR: particle size range in  $\mu\text{m}$ .

LOR: maximum loss on reduction

Table III. Interstitial Impurities of the Starting W Powder

Element	C	Co	Fe	Ni	O	Others
(mg/g)	17	19	14	10	44	97

### 2.2.2. $\text{P}^2\text{C}$ Consolidation Method

For  $\text{P}^2\text{C}$  powder consolidation, a 25.4-mm inner diameter graphite die with a set of top and bottom graphite punches was used. Details of configuration and property data are given by Cho et al., 2005. Fifty grams of powder was loaded into the die; the punch positions were adjusted such that each extended an equal length from either end of the die. To minimize grain growth while maximizing density, the consolidation temperature was set as low as practicable while the applied pressure was set as high as possible with the graphite tooling. The applied pressure, 65 MPa, was limited by the strength of the die. An optimum temperature of  $1700 \text{ }^\circ\text{C}$  at constant

pressure was identified by comparing densities of W compacts consolidated at various temperatures.

### 2.2.3. Precursor Pretreatment

Prior to  $\text{P}^2\text{C}$ , a number of W powder compacts were reduced in flowing  $\text{H}_2$ . Initially, the powder compacts were cold pressed at 27 MPa. The specimen, still held in the graphite die, was inserted into a furnace, heated in  $\text{H}_2$  to  $850 \text{ }^\circ\text{C}$  for 2 hours. The  $\text{H}_2$  flow was turned off when the furnace temperature cooled to  $100 \text{ }^\circ\text{C}$ . Upon removal, a set of punches were inserted into the die and the assembly was immediately loaded into the  $\text{P}^2\text{C}$  vacuum chamber for subsequent consolidation. Alternatively, for W powder compacts without  $\text{H}_2$  reduction, the die assembly was placed directly in the  $\text{P}^2\text{C}$ . In each case, the temperature of the specimen-die assembly was monitored with an optical pyrometer up to  $2000 \text{ }^\circ\text{C}$ . The  $\text{P}^2\text{C}$  vacuum chamber was evacuated to an approximate vacuum level of  $5 \times 10^{-3}$  torr.

Tungsten powder compacts were treated both with and without pulsed current; the on-off cyclic mode of  $\text{P}^2\text{C}$ . Typically, current was applied and incrementally raised at a rate of 200 A every 5 min until it reached 1200 A. In order to avoid possible grain growth during pulsing, the current level was chosen such that the temperature stayed below  $1150 \text{ }^\circ\text{C}$ . The pulsing period was 10 ms on and 10 ms off, with a minimum current level of 0 A. After 5 min at 1200 A, the pressure was increased to 65 MPa. The current was switched to a direct current (DC) mode, and the level was raised from 1200 to 4600 A. Once the pyrometer temperature read  $1700 \text{ }^\circ\text{C}$ , the current was set to 0 A, and the power turned off. For some of the W powder compacts, the DC mode was used throughout. The pressure was increased to 65 MPa and the current increased from 0 to 4600 A. When the pyrometer read  $1700 \text{ }^\circ\text{C}$ , the current was set to 0 A, and the power was turned off. The die assemblies were kept inside of the  $\text{P}^2\text{C}$  apparatus at 65 MPa until the hot zone cooled to  $75 \text{ }^\circ\text{C}$ . The pressure was released and the chamber vented.

The W samples were ejected from the die and densities measured by Archimedes' method. Representative sections of each sample were cut, mounted, and sequentially polished using SiC and diamond. Specimens were etched with Murakami's reagent and examined with X-ray diffraction, SEM, and EDXS.

### 3. RESULTS

#### 3.1. Top-Down Approach

##### 3.1.1. As-Deformed Microstructure

After four ECAP passes, the original W grain size of  $\sim 40 \mu\text{m}$  was refined to a few  $\mu\text{m}$ . The limited grain size reduction was partially attributed to dynamic recrystallization and grain growth at  $1250^\circ\text{C}$ . Figure 1(a) displays the TEM micrograph of UFG W. The average grain size is around  $500 \text{ nm}$ . Note the dislocation cell structure and low angle GBs separating the equiaxed grains. Figure 1(b) displays the typical microstructure of the NC W. The average grain size is about  $100 \text{ nm}$ , but has a high defect density and elongated grain structure. Selected area diffraction analysis of the NC W reveals almost continuous rings, indicative of no texturing.

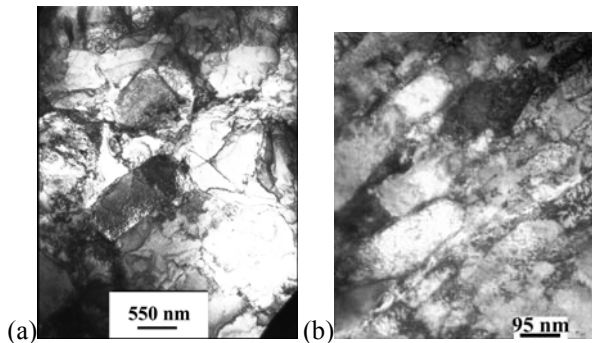


Figure 1. Bright-field TEM images of the (a) UFG-W and (b) NC-W.

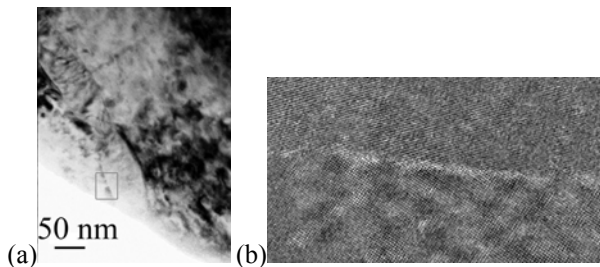


Figure 2. Bright field TEM image of the NC W structure is shown in (a); high-resolution TEM image of the boxed region is shown in (b).

Microstructural analysis revealed that unlike the UFG W, the NC W contains high angle GBs. Shown in Figure 2, lattice images exemplify features such as atomic ledges, steps, and edge dislocations. The presence of atomic facets, steps, or ledges suggests that the NC W is in a high-energy, non-equilibrium state (Valiev et al., 1986; Nazarov et al., 1993; Valiev, 2002). Additionally, no GB phase, amorphous or crystalline, is associated with the GB. That is, the crystalline structure of the constituent grains is disrupted only by the presence of the GB; the GB is clean and well defined. Further

examination also reveals the existence of a large number of edge dislocations near the GBs. This is unusual since W plasticity at low temperatures is usually accommodated by screw dislocations by means a double kink mechanism (Christian, 1983).

##### 3.1.1. Mechanical Behavior

Figure 3 shows the quasi-static and dynamic stress-strain curves of the UFG and NC W specimens. The strength of CG W is about  $1 \text{ GPa}$ ; our results are in agreement with Lennon and Ramesh, 2000, and Dümmer et al., 1998. Note in Figure 3(a) that the UFG W has an increased quasi-static strength of 1.5 times that of CG W. Observe that during deformation the UFG W does not

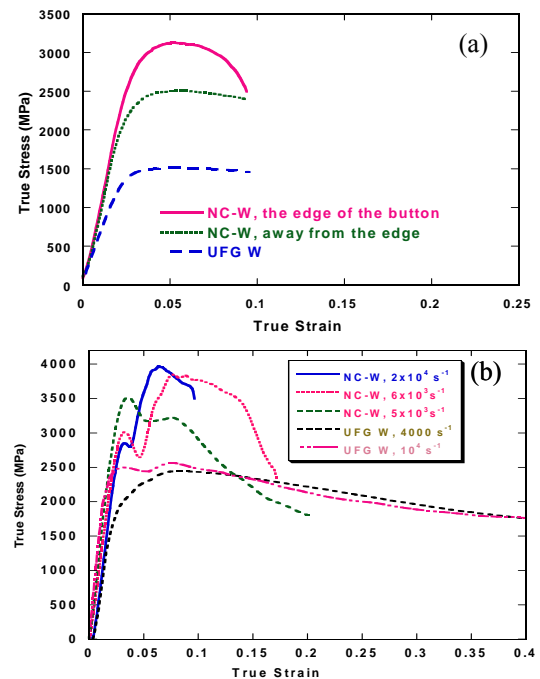


Figure 3. Stress-strain curves of the UFG and NC W under uniaxial compression at quasi-static (a) and dynamic (b) strain rates.

work harden as much. Under dynamic compression, see Figure 3(b), the UFG W shows definite flow softening, even at small plastic strains; in comparison, CG W, even under dynamic loading, continues to strain harden. This flow softening is due to a changed deformation mode. Results for the NC W show a three-fold increase in strength. The strain softening, both at quasi-static and dynamic strain rates, is much more pronounced. This is the most salient feature of the dynamic strain-stress curves: the very early precipitous stress collapse is one of the desirable key properties of a penetrator material (Magness et al., 1995).

### 3.1.2. Failure Behavior

W, subjected to ECAP alone, exhibits axial cracks (i.e., cracks parallel to the loading axis). The cracks are along pre-existing GBs, consistent with the tensile behavior of W, where failure occurs at stress levels about only half that of compression with no evidence of plastic deformation. However, optical microscopy of the post-loaded UFG W (subjected to warm rolling), indicates no axial cracks. Instead, clear evidence of shear bands is observed. An SEM image, shown in Figure 4(a), indicates severe and localized shear deformation. The polished, roughened surface, followed by chemical etching, revealed the detailed microstructure of the shear bands, including the density and direction of the shear lines. The width of the band is around 40  $\mu\text{m}$ . A crack, indicative of incipient failure, can be observed in the middle of the shear band. High-speed photography verified that the stress-collapse in the stress-strain curves roughly corresponds to the initiation of ASBs (Wei et al, 2006a). The strain at which ASBs initiate is around 0.1; they are fully developed at a strain of  $\sim 0.15$ .

Microscopy of the post-loaded NC W indicated a localized shear band at an angle of  $\sim 45^\circ$  with respect to the loading direction. The SEM image, shown in Figure 4(b), displays severe curving of pre-existing surface scratches. In this case, the shear band width is much narrower, about 5  $\mu\text{m}$ . This is significantly smaller than that seen in the UFG W. The cracks form from the highly concentrated shear flow in the band.

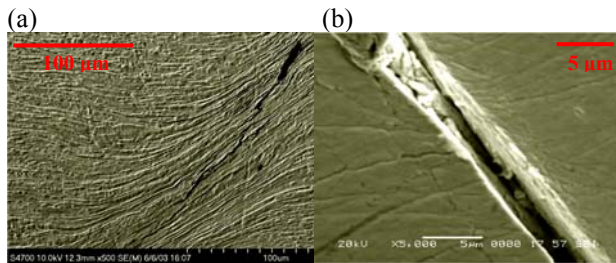


Figure 4. SEM images of (a) UFG W showing severe, localized flow in the shear band; and (b) NC W showing extreme localization and separation.

## 3.2. Bottom-Up Approach

### 3.2.1. Precursor Characteristics

Both particle size and oxygen content of the W powder, as estimated by the vendor, was in good agreement with the experimentally measured oxygen content (see Tables II, III, and IV). However, the oxygen content of the starting powder is significantly higher than the typical 20 ppm level found in wrought W. An SEM image, Figure 5, shows the W powder morphology. The

measured mean particle size of  $\sim 0.7 \mu\text{m}$  indicates that the powder is free of agglomeration.

Table IV. Size Analysis of the W Powder Precursor

	Median ( $\mu\text{m}$ )	Mean ( $\mu\text{m}$ )
Average	0.678	0.702

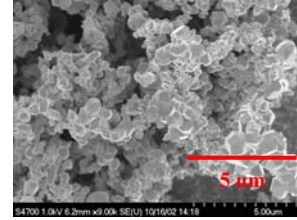


Figure 5. SEM image (SEI) of the starting W powder.

### 3.2.2. Consolidation Characteristics

Results indicated that consolidation above 1700  $^\circ\text{C}$  was hindered by outward deformation of the graphite punches. Such barreling is problematic, as it limits the axial movement into the die and, in turn, densification. This effect caused the density of higher temperature samples to be lower.

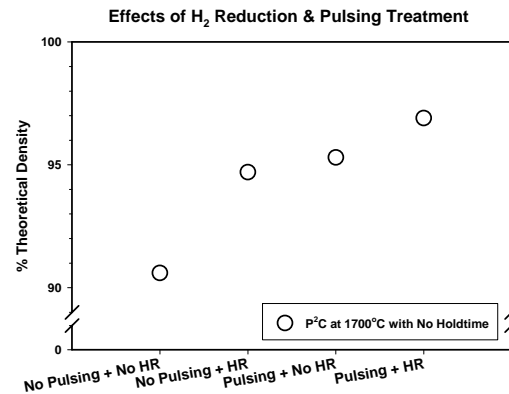


Figure 6. W sample density as a function of  $\text{H}_2$  reduction and current pulsing.

As shown in Figure 6, there are definite benefits to the use of  $\text{H}_2$  reduction and current pulsing: the corresponding W density was higher. Densification was less effective when either one or the other treatments, or no treatment at all was applied. Because of the high oxygen content of the starting powder, a much longer reduction cycle was used than normal. SEM and EDXS, performed on representative sections of the four W samples, all showed oxygen bearing phases, particularly along GBs and at grain-to-grain triple points. Figures 7(a) to (d) display representative backscatter SEM images of the samples. The samples with no treatment, and with reduction or pulsing, only show a larger amount of oxygen containing phases when compared to the sample that had both reduction and pulsing. For all of the W samples, the presence of oxygen was confirmed by EDXS.

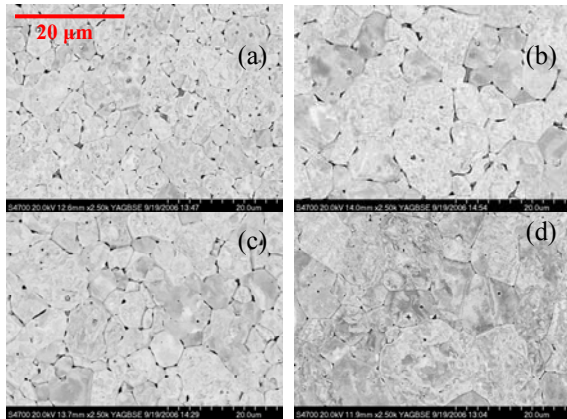


Figure 7. SEM images the W samples: (a) no treatment; (b) H<sub>2</sub> reduction only; (c) pulsing only; and (d) H<sub>2</sub> reduction and pulsing; same magnification in all images.

X-ray diffraction of the precursor powder and densified samples indicated that a tungsten oxide phase was only detected in the starting powder and the W sample without any treatment. It may be noted that the detection limit by X-ray analysis is about 2 vol.%. Therefore, it is possible that the other samples contained tungsten oxide, or other oxide phases, below this detection limit. Careful observation coupled with EDXS analysis revealed that the oxygen containing phase is tungsten oxide. Nevertheless, density measurements clearly indicated an improvement with the dual treatment. As shown in the figure, despite the rapid heating rate of ~400 °C/min and no hold time at the consolidation temperature, the final W grain size was about ten times larger than the initial particle size.

The enhanced densification behavior was a consequence of grain coalescence and growth, suggesting that using a cleaner precursor would be more likely to yield faster densification kinetics. It is hypothesized that for relatively pure precursor powders a heating rate above 1000 °C/min, with a short soak time during potential grain growth, could be applied without degrading W density. However, it must be kept in mind that it is very difficult to process pure UFG or NC W powder to full density without allowing any grain growth at all. Wittmann et al., 2002 and Jain et al., 2006 have suggested the use of grain growth inhibitors to immobilize highly mobile W GBs. Furthermore, these pinning agents should also act as “oxygen” and/or “carbon” getters to deplete residual oxygen and/or carbon during consolidation to effectively reengineer the W GB structure.

#### 4. DISCUSSION

It is well accepted that because of its high density, W is an attractive replacement candidate for depleted uranium kinetic energy penetrators. Unfortunately, because of CG W has a large capacity strain hardening and deforms stably at higher temperatures, it has proven

to be resistant to the development of adiabatic shear localizations despite adiabatic heating developed during the high rate deformation of ballistic impacts. Instead, a uniform stable plastic deformation of CG W penetrators leads to a large mushroomed head on the projectile. This is in contrast to the “self-sharpening” behavior of uranium projectiles, which prevents the build-up of a large head and allows them to burrow narrower but deeper penetration tunnels within armor.

It has been recognized that interstitial impurities such as C, N, S, etc. cause the ceramic-like behavior of CG W (Lassner and Schubert, 1998). Segregation along the GBs renders them into weak links under mechanical straining. Results have shown that single-crystal tungsten can be deformed to significant plastic strain under tension even at liquid nitrogen temperature (Argon and Maloof, 1966). Thus, brittle behavior is not an intrinsic property of W. If these impurities can somehow be depleted, improved ductility could result. An idea by Watanabe, 1984 entails the creation of more GBs with appropriate kinetics to diffuse away impurities from the preexisting GB. If the average impurity concentration is reduced, an increase in GB strength and ductility would follow. A present efficient way to induce more GBs and redistribute impurities is by SPD. As was shown for NC W, the characteristics of the high angle GBs were consistent with this hypothesis. This peculiar feature of the SPD W, explains why significant ductility concurrent with elevated strength was observed.

The high ductility of the SPD W might also be related to the high density of edge dislocations seen with high-resolution TEM. Factors controlling fracture toughness and brittle-to-ductile transition of W indicates that pre-plastic-deformation of the specimen can increase both low- and high-temperature fracture toughness (Gumbsch, et al., 1998). It is pointed out that a dislocation moving in the stress field along a crack tip will generate highly mobile non-screw-type dislocation segments parallel to the crack tip. Our high-resolution TEM showed residual edge dislocations in NC W.

A shear susceptibility model can be articulated to predict the propensity of the UFG and NC W for ASB. The enhanced propensity for shear banding of UFG and NC W samples could be explained in terms of the Wright criterion (Wright, 2002). The susceptibility is directly proportional to the thermal softening and yield strength, while inversely proportional to density, specific heat, strain hardening exponent, and the SRS. For a perfectly plastic material (no strain hardening) such as the UFG and NC W, the critical parameters are the yield strength and the SRS. A large yield strength will translate into higher susceptibility. Furthermore, a small SRS also results in a higher susceptibility. Recent results on UFG/NC BCC metals have shown that the SRS is considerably reduced

compared to the CG microstructure (Wei et al., 2004c). A simple calculation based on the experimental results and the physical properties of W shows that susceptibility of the UFG and NC W is several orders of magnitude higher than that of conventional CG W.

## 5. SUMMARY

The current work has demonstrated a strategy to induce highly localized shear flow in W. This is based on refining the microstructure down to UFG and NC scale using SPD. Microstructural and mechanical property analyses of UFG- and NC-W processed by SPD have led to the hypothesis that grain refinement, depletion, and redistribution of pre-existing impurities segregated along the GBs are the critical aspects for inducing flow softening while improving the material ductility.

SPD results have been used to aid the design of consolidation experimental parameters as well. To date, a density of 97% theoretical has been achieved by using H<sub>2</sub> reduction and current pulsing to remove residual oxygen on the starting W powder. Microstructural examination has revealed that oxygen containing phases still remain in the P<sup>2</sup>C-consolidated W samples, particularly at W GBs and at triple points. Samples consolidated without treatment contain much higher levels of tungsten oxides. Based on these experiments, it may be concluded that if finer nanosized W powders become available, the final W grain size will be about an order of magnitude greater. As shown by the SPD results, the required final grain size of about 100 to 500 nm will only be reached with a combination of high purity W nanopowders and appropriate grain growth inhibitors.

## REFERENCES

- Argon, A.S. and Maloof, S.R., 1966: Plastic Deformation of Tungsten Single Crystals at Low Temperature, *Acta Mater*, **14**, 1449-1462.
- Bai, Y. and Dodd, B., 1992: *Adiabatic Shear Localization*. Pergamon Press.
- Carsley, J.E., Fisher, A., Milligan, W.W., and Aifantis, E.C., 1998: Mechanical Behavior of Bulk Nanostructured Iron Alloy, *Metall. Mater. Trans. A*, **29**, 2261-2271.
- Cheng S., Ma, E., Wang, Y.M., Kecskes, L.J., Youssef, K.M., Koch, C.C., Trociewitz, U.P., and Han, K., 2005: Tensile Properties of in-situ Consolidated Nanocrystalline Copper with a Narrow Grain Size Distribution, *Acta Mater.*, **53**, 1521-1533.
- Cho, K.C., Woodman, R.H., Klotz, B.R., and Dowding, R.J., 2004: Plasma Pressure Compaction of Tungsten Powders, *Mater. Manuf. Processes*, **19**, 619-630.
- Cho, K., Kellogg, F., Klotz, B.R., and Dowding, R.J., 2005: Plasma Pressure Compaction of Submicron Size Tungsten Powder, *Proc., Sixth Int. Conf. On Tungsten, Refractory & Hardmetals VI*, Orlando, FL, Metal Powder Industries Federation, CD-ROM, 161-170.
- Christian, J.W., 1983: Some Surprising Features of the Plastic-Deformation of Body-Centered Cubic Metals and Alloys, *Metall. Trans. A*, **14**, 1237-1256.
- Dümmer T., LaSalvia, J.C., Ravichandran, G., and Meyers, M.A., 1998: Effects of Strain Rate on Plastic Flow and Failure in Polycrystalline Tungsten, *Acta Mater*, **46**, 6267-6290.
- Groza, J.R., 1998: *Field-activated Sintering*, ASM Handbook; Powder Metallurgy, Vol. 7, ASM International, 583 pp.
- Gumbsch, P., Riedle, J., Hartmaier, A., and Fischmeister, H.F., 1998: Controlling Factors for the Brittle-to-Ductile Transition in Tungsten Single Crystals, *Science*, **282**, 1293-1295.
- Farrell, K., Schaffhauser, A.C., and Stiegler, J.O., 1967: Recrystallization, Grain Growth and the Ductile-Brittle Transition in Tungsten Sheet, *J. Less Common Metals*, **13**, 141-155.
- Jain, M., Skandan, G., Martin, K., Kapoor, D., Cho, K., Klotz, B., Dowding, R., Agarawal, D., and Cheng, J., 2006: Microwave Sintering: A New Approach to Fine-Grain Tungsten-II, *Int. J. Powder Metall.*, **42**, 53-57.
- Jia, D. and Ramesh, K.T., 2004: A Rigorous Assessment of the Benefits of Miniaturization in the Kolsky Bar System, *Exp. Mech.*, **44**, 445-454.
- Jia, D., Ramesh, K.T., and Ma, E., 2003: Effects of Nanocrystalline and Ultrafine Grain Sizes on Constitutive Behavior and Shear Bands in Iron, *Acta Mater*, **51**, 3495-3590.
- Jonas, J.J., Holt, R.A., Coleman, C.E., 1976: Plastic Instability in Tension and Compression, *Acta Metall.*, **24**, 911-918.
- Lennon, A.M. and Ramesh, K.T., 2000: The Thermoviscoplastic Response of Polycrystalline Tungsten in Compression, *Mater. Sci. Eng., A*, **276**, 9-21.
- Koch, C.C., 2003: Optimization of Strength and Ductility of Nanocrystalline and Ultrafine Grained Metals, *Scripta Mater.*, **49**, 663-668.
- Kumar, K.S., Van Swygenhoven, H., Suresh, S., 2003: Mechanical Behavior of Nanocrystalline Metals and Alloys, *Acta Mater.*, **51**, 5743-5774.
- Lassner, E. and Schubert, W.D., 1998: *Tungsten: Properties, Chemistries, Technology of the Element, Alloys, and Chemical Compounds*, Kluwer Academic / Plenum Publishers.
- Ma, E., 2003a: Instabilities and Ductility of Nanocrystalline and Ultrafine-Grained Metals, *Scripta Mater.*, **49**, 663-668.
- Ma, E., 2003b: Controlling Plastic Instability, *Nature Materials*, **2**, 7-8.
- Magness L.S., Kapoor, D., and Dowding, R., 1995: Novel Flow-Softening and Flow-Anisotropy Approaches to

- Developing Improved Tungsten Kinetic Energy Penetrator Materials, *Mater. Manuf. Processes*, **10**, 531-540.
- Malow T.R., and Koch, C.C., 1998: Mechanical Properties in Tension of Mechanically Attrited Nanocrystalline Iron by the Use of Miniaturized Disk Bend Test, *Acta Mater.*, **46**, 6459-6473.
- Malow T.R., Koch, C.C., Miraglia, P.Q., and Murty, K.L., 1998: Compressive Mechanical Behavior of Nanocrystalline Fe Investigated with an Automated Ball Indentation Technique, *Mater. Sci. Eng., A*, **252**, 36-43.
- Meyers M.A., Mishra, A., and Benson, D.J., 2006: Mechanical Properties of Nanocrystalline Materials, *Prog. Mater. Sci.*, **51**, 427-556.
- Nazarov, A.A., Romanov, A.E., and Valiev, R.Z., 1993: On the Structure, Stress Field and Energy of Nonequilibrium Grain Boundaries, *Acta Metall. et Mater.*, **41**, 1033-1040.
- Rieck, G.D., 1967: *Tungsten and Its Compounds*, Pergamon Press.
- Valiev, R.Z., 2002: Nanomaterial Advantage, *Nature*, **419**, 11-56.
- Valiev, R.Z., Gertsman, V.Y., and Kaibyshev, R., 1986: Grain Boundary Structure and Properties Under External Influence, *Phys. Status Solidi A*, **97**, 11-56.
- Valiev, R.Z., Islamgaliev, R.K., and Alexandrov, I.V., 2000: Bulk Nanostructured Materials from Severe Plastic Deformation, *Prog. Mater. Sci.*, **45**, 103-189.
- Valiev, R.Z., Alexandrov, I.V., Zhu, Y.T., and Lowe, T.C., 2002: Paradox of Strength and Ductility in Metals Processed by Severe Plastic Deformation, *J. Mater. Res.*, **17**, 5-8.
- Wang, Y.M. and Ma, E., 2004: Three Strategies to Achieve Uniform Tensile Deformation in a Nanostructured Metal, *Acta Mater.*, **52**, 1699-1709.
- Wang, Y.M., Chen, M.W., Zhou, F.H., and Ma, E., 2002: High Tensile Ductility in Nanostructured Metal, *Nature*, **419**, 912-915.
- Watanabe, T., 1984: An Approach to Grain Boundary Design for Strong and Ductile Polycrystals, *Res Mechanica*, **11**, 47-84.
- Wei Q., Jia, D., Ramesh, K.T., and Ma, E., 2002: Evolution and Microstructure of Shear Bands in Nanostructured Fe, *Appl. Phys. Lett.*, **81**, 1240-1242.
- Wei, Q., Jiao, T., Mathaudhu, S.N., Ma, E., Hartwig, K.T., and Ramesh, K.T., 2003: Microstructure and Mechanical Properties of Tantalum After Equal Channel Angular Extrusion (ECAE), *Mater. Sci. Eng., A*, **358**, 266-272, 2003.
- Wei, Q., Kecskes, L.J., Jiao, T., Hartwig, K.T., Ramesh, K.T., and Ma, E., 2004a: Adiabatic Shear Banding in Ultra Fine Grained Fe Processed by Severe Plastic Deformation, *Acta Mater.*, **52**, 1859-1869.
- Wei, Q., Jiao, T., Ramesh, K.T., and Ma, E., 2004b: Nanostructured Vanadium: Processing and Mechanical Properties under Quasi-static and Dynamic Compression, *Scripta Mater.*, **50**, 359-364.
- Wei, Q., Cheng, S., Ramesh, K.T., and Ma, E., 2004c: Effects of Nanocrystalline and Ultrafine Grain Sizes on the Strain Rate Sensitivity and Activation Volume: FCC versus BCC Metals, *Mater. Sci. Eng., A*, **381**, 71-79.
- Wei, Q., Jiao, T., Ramesh, K.T., Ma, E., Kecskes, L.J., Magness, L., Dowding, R.J., Kazykhanov, V.U., and Valiev, R.Z., 2006a: Mechanical Behavior and Dynamic Failure of High-Strength Ultrafine Grained Tungsten Under Uniaxial Compression, *Acta Mater.*, **54**, 77-87.
- Wei, Q., Schuster, B.E., Ramesh, K.T., Kecskes, L.J., Dowding, R.J., Cho, K.C., Magness, L., Ma, E., Ramesh, K.T., and Valiev, R.Z., 2006b: Nanoengineering Applied to Tungsten, *Proc., Sixth Int. Conf. on Tungsten, Refractory & Hardmetals VI*, Orlando, FL, Metal Powder Industries Federation, CD-ROM, 216-225.
- Wei, Q., Zhang, H.T., Schuster, B.E., Ramesh, K.T., Valiev, R.Z., Kecskes, L.J., Dowding, R.J., Magness, L., and Cho, K., 2006c: Microstructure and Mechanical Properties of Super-Strong Nanocrystalline Tungsten Processed by High-Pressure Torsion, *Acta Mater.*, **54**, 4079-4089.
- Witkin, D.B., and Lavernia, E.J., Synthesis and Mechanical Behavior of Nanostructured Materials via Cryomilling, *Prog. Mater. Sci.*, **51**, 1-60.
- Wittmann, B., Schubert, W.D., and Lux, B., 2002: WC Grain Boundary and Grain Growth Inhibition in Nickel and Iron Binder Hardmetals, *Int. J., Refract. Met. Hard Mater.*, **20**, 51-60.
- Wright, T.W., 2002: *The Physics and Mathematics of Adiabatic Shear Bands*, Cambridge Press.
- Yoo, S.H., Sethuram, K.M., and Surdarshan, T.S., 1999: *Apparatus for Bonding Particle Materials to Near Theoretical Density*, U.S. Patent No. 5,989,487.
- Youssef, K.M., Scattergood, R.O., Murty, K.L., Horton, J.A., and Koch, C.C., 2004: Ultrahigh Strength and High Ductility of Bulk Nanocrystalline Copper, *Appl. Phys. Lett.*, **87**, 091904-1-091904-3.
- Zhilyaev, A.P., Lee, S., Nurislamova, G.V., Valiev, R.Z., and Langdon, T.G., 2001: Microhardness and Microstructural Evolution in Pure Nickel During High-Pressure Torsion, *Scripta Mater.*, **44**, 2753-2758.
- Zhilyaev, A.P., Nurislamova, G.V., Kim, B.K., Baro, M.D., Szpunar, J.A., and Langdon, T.G., 2003: Experimental Parameters Influencing Grain Refinement and Microstructural Evolution During High-Pressure Torsion, *Acta Mater.*, **51**, 753-765.

NO. OF  
COPIES ORGANIZATION

1 DEFENSE TECHNICAL  
(PDF INFORMATION CTR  
ONLY) DTIC OCA  
8725 JOHN J KINGMAN RD  
STE 0944  
FORT BELVOIR VA 22060-6218

1 US ARMY RSRCH DEV &  
ENGRG CMD  
SYSTEMS OF SYSTEMS  
INTEGRATION  
AMSRD SS T  
6000 6TH ST STE 100  
FORT BELVOIR VA 22060-5608

1 DIRECTOR  
US ARMY RESEARCH LAB  
IMNE ALC IMS  
2800 POWDER MILL RD  
ADELPHI MD 20783-1197

3 DIRECTOR  
US ARMY RESEARCH LAB  
AMSRD ARL CI OK TL  
2800 POWDER MILL RD  
ADELPHI MD 20783-1197

ABERDEEN PROVING GROUND

1 DIR USARL  
AMSRD ARL CI OK TP (BLDG 4600

NO. OF  
COPIES ORGANIZATION

ABERDEEN PROVING GROUND

59 DIR USARL  
AMSRD ARL WM RP  
E RIGAS  
AMSRD ARL O AP EG  
M ADAMSON  
AMSRD ARL WM M  
CHIEF  
R DOWDING  
J MCCAULEY  
AMSRD ARL WM MA  
CHIEF  
AMSRD ARL WM MB  
CHIEF  
K CHO  
J BENDER  
T BOGETTI  
J BROWN  
L BURTON  
R CARTER  
W DRYSDALE  
R EMERSON  
D GRAY  
D HOPKINS  
R KASTE  
E KLIER  
L KECSKES  
H MAUPIN  
M MINNICINO  
B POWERS  
D SNOHA  
J SOUTH  
M STAKER  
J SWAB  
J TZENG  
AMSRD ARL WM MC  
CHIEF  
R BOSSOLI  
S CORNELISON  
D GRANVILLE  
B HART  
M MAHER  
F PIERCE  
W SPURGEON  
AMSRD ARL WM MD  
CHIEF  
B CHEESEMAN  
P DEHMER  
R DOOLEY  
G GAZONAS  
S GHIORSE  
M KLUSEWITZ  
J LASALVIA  
J MONTGOMERY

NO. OF  
COPIES ORGANIZATION

J SANDS  
D SPAGNUOLO  
S WALSH  
AMSRD ARL WM TA  
CHIEF  
M BURKINS  
B GOOCH  
AMSRD ARL WM TC  
CHIEF  
R COATES  
L MAGNESS  
B SCHUSTER  
AMSRD ARL WM TD  
CHIEF  
D DANDEKAR  
M RAFTENBERG  
T WEERASOORIYA